Journal of Institute of Science and Technology, 30(2), 55-64 (2025)
ISSN: 2467-9062 (print), e-ISSN: 2467-9240
https://doi.org/10.3126/jist.v30i2.82535

Research Article

MECHANICAL, THERMAL, AND OPTICAL PROPERTIES OF $MoTe_2$ AND $MoSe_2$ MONOLAYER TMDCS MATERIALS: FIRST-PRINCIPLES STUDY

Tejendra Neupane[1], Arpan Pokharel[1], Kamal Khanal[1], Sukrit Kumar Yadav[1], Ganesh Paudel[1], Om Shree Rijal[1], Hari Krishna Neupane[1]*

[1]Amrit Campus, Institute of Science and Technology, Tribhuvan University, Kathmandu Nepal
**Correspondence: hari.neupane@ac.tu.edu.np*

(Received:** July 30, 2025; **Revised:** November 05, 2025; **Accepted:** November 15, 2025**)

ABSTRACT

Materials can be used in the fields of electronic, optoelectronics, and thermoelectric devices based on their electronic, optical, mechanical and thermal properties. In this study, we explored the mechanical, thermal, and optical properties of $MoSe_2$ and $MoTe_2$ materials computationally, using density functional theory (DFT) method through quantum ESPRESSO computational software package. For the investigation of materials mechanical properties, their elastic constants and modulus of rigidities are analyzed. It is found that $MoSe_2$ and $MoTe_2$ have brittle, soft, and compressible properties. Both have anisotropic tendencies as suggested by Chung-Buessem anisotropic ratio. Phonon velocities, and Debye temperature of $MoSe_2$ and $MoTe_2$ are examined for the prediction of their thermal properties. Both materials have good thermal properties. Complex dielectric function has been deployed for the analysis of materials optical properties. The nature of different optical curves such as optical conductivity, absorption coefficient, transmission coefficient, and reflection coefficient (reflectivity) is studied from complex dielectric functions and found that both materials have optical anisotropy nature with greater degree of polarization in xx- & yy- plane than in zz-plane. Moreover, materials have semiconducting properties based on their absorption coefficient plots. They also have higher transmission occurred at low energy region (up to 1.2 eV), and higher absorption values at energy range (1.10 - 3.5) eV. The results suggest that $MoSe_2$ and $MoTe_2$ materials can be used as effective absorbent materials in the infrared and visible light regions. Hence, these materials can be used to create more efficient photoelectronic as well as optoelectronic devices.

Keywords: Anisotropy, Conductivity, DFT, Dynamical, Monolayer

INTRODUCTION

We live in a technological era in which new and advanced materials are being developed continuously. Among these, two-dimensional (2D) materials are of great importance because of their unique properties and potential applications in electronics, optoelectronics and various other emerging fields (Chang *et al.*, 2016; Novoselov *et al.*, 2005; Tsai *et al.*, 2014; Wang *et al.*, 2012). The transition metal dichalcogenides (TMDCs) have shown great promise and rightly capture the interest of today's researchers. This is because these materials have been successfully used in various applications like solar cells, smartphones, biomedicine, lubricants to name a few (Mia *et al.*, 2023; D'angelo & Matsuda, 2019; Pumera, 2014). Among the various types of TMDCs materials, Mo-based materials are promising candidates in the field of optoelectronic and spintronic devices. Current research has shown that monolayer MoX_2 (X= S, Se, Te) materials can exist in stable state in hexagonal phase (Brown, 1966; Puotinen & Newnham, 1961). These materials have one Mo-atom in between two X-atoms (X= chalcogens) (Kuc *et al.*, 2015; Mia *et al.*, 2023). Moreover, monolayers of Mo-based materials have a tunable direct band gap ranging from 1.10 eV to 1.60 eV (Ma *et al.*, 2011; Ruppert *et al.*, 2014; Tongay *et al.*, 2012; Vellinga *et al.*, 1970). Due to this moderate direct band gap, the development of high-end semiconductors and various optoelectronic devices become possible using these materials (Luo *et al.*, 2022; Pumera, 2014). Moreover, tunability of magnetic properties (from factor like doping, defect, and layer stacking) of these materials make them excellent in the fields of optoelectronic and spintronics devices (Aryal *et al.*, 2025; Baithi *et al.*, 2024; Kanoun, 2018; Neupane *et al.*, 2020; Paudel *et al.*, 2023;). Moreover, due to their 2D nature, they can be successfully exploited in nanotechnology. They can be used in the field of biotechnology and biomedicine (; Kumar *et al.*, 2025; Nepal *et al.*, 2024; Mia *et al.*, 2023; Neupane & Adhikari 2021). Due to the massive potential of these monolayer compounds, it is essential to accurately understand about their complex dielectric functions (ε_1 & ε_2). This is important because all other optical constants can be derived from the complex dielectric function. This in turn helps one understand optical properties of material. Mechanical as well as

optical properties for bulk and heterojunctions of $MoTe_2$ and $MoSe_2$ have been reported (Li *et al.*, 2021; Luo *et al.*, 2022; Rassay, 2017). However, these properties have not yet been computationally investigated for supercell configurations of monolayer $MoTe_2$ and $MoSe_2$ using the GGA: PBE functional, which constitutes the primary motivation for the present study. Moreover, the detailed analyses such as $\varepsilon_1/\varepsilon_2$ components, thermal parameters, and property variations under supercell expansion remain unexplored. This gap forms the main motivation of the present work. Therefore, we investigated the mechanical, thermal, and optical properties of (3×3) supercell monolayers of $MoTe_2$ and $MoSe_2$ materials using density functional theory (DFT) method with Quantum ESPRESSO as computational tool.

MATERIALS AND METHODS

Spin-polarized DFT calculations were performed to investigate the electronic structure of monolayer $MoTe_2$ and $MoSe_2$ (Bartolotti & Flurchick, 1996; Giustino, 2014; Orio *et al.*, 2009). Plane-wave basis set together with ultrasoft pseudopotential (USPP) has been used under computational tool Quantum ESPRESSO (QE) for data optimization (Dal Corso, 1996; Kokalj, 2003**).** Two software packages, namely XmGrace and XcrySDen are utilized as graph plotting and crystal visualization tools, which made our work easier and faster (Kokalj, 2003). Exchange-correlation energy was calculated using the Perdew-Burke-Ernzerhof (PBE) functional within the generalized gradient approximation (GGA) approach (Kohn & Sham, 1965; Van Voorhis & Scuseria, 1998). First, the optimized unit cells of $MoTe_2$ and $MoSe_2$ are prepared by introducing a vacuum layer of 20 Å thickness to prevent any unphysical interactions along the z-direction. For this, all of the required parameters (i.e., K-points, energy cutoff, and lattice parameters) have been optimized and calculated. These optimizations are performed using self-consistent calculations. The values of lattice constant (a) are calculated to be 5.90 Å of $MoTe_2$, and 5.83 Å of $MoSe_2$, while deploying (8×8×1) Monkhorst-Pack K-points grid (Wang *et al.*, 2021). The reciprocal space (Brillouin zone**)** is sampled using "Γ" centric grid for easy and efficient calculations. The kinetic energy cutoff (ecutwfc) of plane waves is found to be 50.71 Ry and 34.61 Ry for $MoTe_2$ and $MoSe_2$. Then, the materials used are made into supercell monolayer structures. These structures are obtained by the expansion of two-dimensional (2D) unit cells in x and y directions after which the structures are relaxed again. Thereafter, the data obtained are used to study the mechanical, thermal, and optical properties of these materials. Mechanical and thermal properties of $MoTe_2$, and $MoSe_2$ are studied using Voight, Reuss and Hill methods (Al-Qaisi *et al.*, 2017) methods and then estimated the elastic constants and modulus (Young modulus, shear modulus and bulk modulus) rigidity of the considered materials. Values of Debye temperature (θ_D), and average phonon velocities (v_{avg}) are essential for the determination of material thermal properties. The dielectric function (ε) is analyzed in great detail for the study of materials optical properties using time-dependent ground state perturbation theory under random phase approximation (RPA) (Korner & Elsasser, 2010).

RESULTS AND DISCUSSION

We interpretated the mechanical, thermal, and optical properties of (3×3) supercell structures of MoX_2 (X= Se, Te) materials, and compared their findings with the available reported works.

Mechanical Properties

We studied mechanical properties of $MoTe_2$ and $MoSe_2$ materials, which are shown in Figures-1(a & b) respectively.

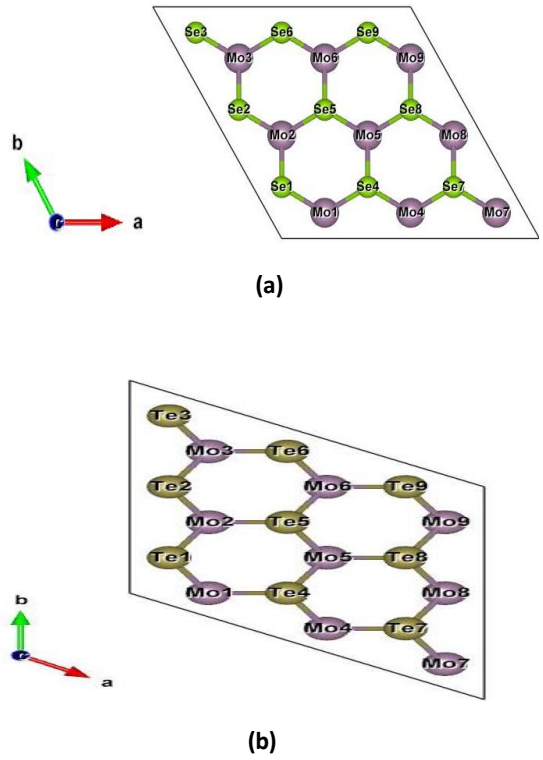

Figure 1. (Color online) (a) Front view of (3×3) supercell structure of $MoSe_2$ monolayer, and (b) Front view of (3×3) supercell structure of $MoTe_2$ monolayer.

We studied the mechanical properties to understand the mechanical behavior and stability of the considered $MoTe_2$ and $MoSe_2$ monolayers. These elastic constants

verify the mechanical stability of solid materials using Born stability criteria (Mouhat & Coudert, 2014);

$C_{11} > 0$
$C_{33} > 0$
$C_{44} > 0$
$C_{11} - C_{12} > 0$
$(C_{11} + C_{12})C_{33} > 2C_{13}^2$
$C_{66} = \frac{C_{11} - C_{12}}{2} > 0$.

These elastic constants (C_{ij}) are calculated by using Voight, Reuss and Hill methods (Al-Qaisi *et al.*, 2017). Monolayer $MoTe_2$ and $MoSe_2$ have hexagonal structures and six different elastic constants namely C_{11}, C_{12}, C_{13}, C_{33}, C_{44} and C_{66}. Among them C_{66} is dependent which is calculated as $C_{66} = (C_{11}-C_{12})/2$. For considered materials having hexagonal structure, they satisfied the above inequalities criteria. Hence, the $MoTe_2$ and $MoSe_2$ are mechanically stable materials. Additionally, mechanical properties of these materials are explored by analyzing their estimated values of modulus of rigidity. Mechanical property is the behavior of a material under external force. This is useful in understanding characteristics such as hardness or softness, brittleness or ductility etc. nature of the materials. We found that both $MoTe_2$ and $MoSe_2$ belong to P6m2 point group and hexagonal system. Here, P is the primitive lattice, 6 is six-fold inversion axis, m is for mirror plane and 2 denotes two-fold rotation axis, which is perpendicular to 6-fold axis. We have used Voight, Reuss and Hill methods to calculate the various elastic moduli. Values obtained from Hill method are arithmetic average of the Voight and Reuss values and is more accurate than other two. This is because Voight method gives upper limit of a parameter while Reuss method gives lower limit. The various formulas are given below (Al-Qaisi *et al.*, 2017);

$$B_v = \frac{2(C_{11} + C_{12}) + 4C_{13} + C_{13}}{9} \dots (1)$$

$$S_v = \frac{C_{11} + C_{12} + 2C_{33} + 12C_{44} + 12C_{66} - 4C_{13}}{30} \dots (2)$$

where, B_v and S_v are Bulk and Shear modulus calculated by Voight method. Bulk and Shear modulus are calculated by Reuss method are (Al-Qaisi *et al.*, 2017; Reuss, 1929);

$$B_R = \frac{C_{33}(C_{11} + C_{12}) - 2C_{12}^2}{C_{11} + C_{12} + 2C_{33} - 4C_{13}} \dots (3)$$

$$S_R = \frac{5[C_{33}|(C_{11} + C_{12}) - 2C_{12}^2]C_{55}C_{66}}{2[3B_vC_{55}C_{66} + C_{33}(C_{11} + C_{12}) - 2C_{12}^2(C_{55}+C_{66})]} \dots (4)$$

Young's modulus is estimated by Hill method using equation-(5) (Al-Qaisi *et al.*, 2017);

$$Y = \frac{9B_HS_H}{3B_H+S_H} \dots (5)$$

where, B_H and S_H are respectively represented by Bulk and Shear modulus of rigidities. From the above formulas, we have estimated the modulus of rigidities of materials, which are summarized in a table-1. We note that both $MoTe_2$ and $MoSe_2$ exhibits the equal value for most mechanical parameters. This may be due to their equal band gaps and similar lattice structures. From the above calculations, we have calculated Bulk modulus (*B*) of $MoTe_2$ and $MoSe_2$ to be 10.789 GPa, which is comparable values of diamond reported in the literatures (Cohen, 1985; Chen *et al.*, 2016). Hence, both monolayer materials are easy to compress. Shear (*S*), and Young's modulus (*Y*) are used to study hardness and stiffness of a material. Materials with larger Young's modulus values exhibit greater stiffness. The relatively small value of *Y* (16.67 GPa for both materials) shows that the materials can't handle large tensile stress as the value of (10-100) GPa falls under moderately stiff material (Chen *et al.*, 2016). This result is also supported by Vickers hardness coefficient of materials which is equal to 2.06 GPa for both $MoTe_2$ and $MoSe_2$ materials. Moreover, higher value of *S* means, material will be more resistant to shape change (Al-Qaisi *et al.*, 2017). But, the value of 6.70 GPa suggests low resistance to change the shape. These values reveal that the materials are soft and moderately stiff. This result is also supported by the value of P-wave modulus. We also calculated Poisson ratio (ν) by using Equation -6 (Al-Qaisi *et al.*, 2017);

$$\nu = \frac{3B_H-2S_H}{2(3B_H+S_H)} \dots (6)$$

Moreover, it is important to understand brittleness or ductility of a material. If a material is ductile, it can deform significantly before breaking. However, brittle materials break more easily. To study this nature, we have used Poisson's ratio as well as Pugh's ratio of considered materials. If Poisson's ratio (ν) > 0.26, and Pugh's ratio >1.75, materials are said to be ductile otherwise brittle (Rijal *et al.*, 2025). The calculated values of Poisson's ratio (ν) for $MoTe_2$ and $MoSe_2$ are found to be 0.24 and 0.24, respectively, while the corresponding Pugh's ratios are 1.60 for $MoTe_2$ and 1.61 for $MoSe_2$. This indicates that $MoTe_2$ and $MoSe_2$ are brittle in nature. The calculated values of Poisson's ratio and Pugh's ratio for the considered materials agree with previously reported values of other compounds (Zeng *et al.*, 2015). The Poisson's ratio and Pugh's ratio are also used to study lateral expansion of a material to longitudinal strain. The value of ν > 0 implies the material expands laterally

when it is longitudinally stretched and this is true for our materials. Similarly, the isotropic or anisotropic nature of materials depends on the value of Chung-Buessem anisotropy index (A). If the calculated value (A) is equal to 1, the material is isotropic; otherwise, it is anisotropic. In our case for $MoTe_2$ and $MoSe_2$, the calculated (A) value is 1.10, which is greater than 1. Its reveals that both $MoTe_2$ and $MoSe_2$ materials have anisotropic properties. The calculated (A) values of the considered compounds fairly agree with previously reported values of other materials (Lin *et al.*, 2025). The Chung-Buessem anisotropy is estimated by using equation -(7) (Al-Qaisi *et al.*, 2017; Pathak, 2019);

$$A = \frac{\mu_v - \mu_R}{\mu_v + \mu_R} \ldots (7)$$

where, μ_v = Average value of Shear modulus calculated using Voight method and μ_R = Reuss average of Shear modulus. The Kleinman parameter (ζ) reflects the relative ease of bond bending versus bond stretching in the material, with values closer to 0 indicating dominant bond bending and values near 1 indicating dominant bond stretching. Our estimated value of ζ = 0.50, which implies that considered materials have bond bending and bond stretching contribute equally to the deformation. So, if $\zeta = 0.5$, it indicates that the material deforms through a balanced combination of bond bending and bond stretching, with neither mechanism dominating.

Table 1. The parameters for the investigation of materials mechanical properties are calculated using Voight, Reuss and Hill methods.

Mechanical parameters	Voight		Reuss		Hill	
	$MoTe_2$	**$MoSe_2$**	**$MoTe_2$**	**$MoSe_2$**	**$MoTe_2$**	**$MoSe_2$**
Bulk modulus (B)	21.72 GPa	21.73 GPa	0.14 GPa	0.14 GPa	10.79 GPa	10.79 GPa
Young's Modulus (Y)	34.19 GPa	34.22 GPa	0.61 GPa	0.61 GPa	16.67 GPa	16.67 GPa
Shear Modulus (*S*)	13.81 GPa	13.83 GPa	0.40 GPa	0.40 GPa	6.70 GPa	6.70 GPa
Poisson's Ratio (*v*)	0.24	0.24	0.23	0.24	0.24	0.24
Pugh's Ratio ($\frac{B}{S}$)	1.57	1.57	0.35	0.35	1.60	1.61
Vickers Hardness	-	-	-	-	2.06 GPa	2.06 GPa
P-wave Modulus	40.14 GPa	-0.68 GPa	19.73 GPa	40.14 GPa	-0.68 GPa	19.73 GPa
Kleinman Parameter (ζ)	0.50	0.50				
Chung-Buessem Anisotropy (*A*)	1.10	1.10				

Thermal Properties

The materials thermal properties are analyzed on the basis of calculated values of phonon velocities and Debye temperature. The average phonon velocity (V_m), and Debye temperature (θ_D) are calculated by using equation-(8 & 9) (Komatitsch *et al.*, 1999; Anderson, 1963);

$$v_m = \left[\frac{1}{3}\left(\frac{2}{v_t^3} + \frac{1}{v_l^3}\right)\right]^{\frac{-1}{3}} \ldots (8)$$

$$\theta_D = \frac{h}{k_B}\left[\frac{3N}{4\pi}\frac{\rho N_A}{M}\right]^{\frac{1}{3}} v_m \ldots (9)$$

where, h = Planck's constant, k_B = Boltzmann constant, M = Molar mass, ρ = Density, and N_A = Avogadro's number. The calculated values of longitudinal velocity, transverse velocity, average velocity, and Debye temperature for $MoTe_2$ and $MoSe_2$ materials are listed in table-2. The values of average velocity (v_m) and Debye temperature (θ_D) suggest that the materials have low phonon velocity and low melting point (Han *et al.*, 2025). The calculated (θ_D) for $MoSe_2$ and $MoTe_2$ are found to be 135.2 K and 114.9 K, respectively. The calculated (θ_D) values are in good agreement with those reported for other TMDCs materials (Nakamura, 2018). The greater (θ_D) of $MoSe_2$ implies these materials have stronger inter atomic bonds and better thermal conductivity compared to $MoTe_2$. Moreover, this also suggests that phonon velocity is higher and specific heat capacity is greater in monolayer $MoSe_2$ than $MoTe_2$. Similarly, a lower Debye temperature indicates weaker interatomic bonding. So, the bond strength is stronger in monolayer $MoSe_2$.

Table 2. Estimated values of thermal parameters like Debye temperature (θ_D), average phonon wave velocity (v_m) of monolayer $MoTe_2$ and $MoSe_2$.

Parameters	Value	
	$MoTe_2$	**$MoSe_2$**
Longitudinal Wave Velocity (v_l)	2095.70 m/s	2465.50 m/s
Transverse Wave Velocity (v_t)	1221.83 m/s	1437.63 m/s
Average Velocity (v_m)	1355.29 m/s	1594.63 m/s
Debye Temperature (θ_D)	114.90 K	135.20 K

Optical Properties

In this study, we examined the optical conductivity, absorption coefficient, transmittance coefficient, reflectivity coefficient, and the real and imaginary parts of dielectric function of $MoTe_2$ and $MoSe_2$ materials.

Dielectric Function

The optical properties of materials are predicted based on their complex dielectric function ε(ω), that describes material polarization response to external electric field. The reason for the complex form is due to causal response of the material to applied field. Due to this reason, ε(ω) can be written as (Lawaetz, 1972);

$$\varepsilon(\omega) = \varepsilon_1(\omega) + i\varepsilon_2(\omega) \ldots (10)$$

Here, the real part $\varepsilon_1(\omega)$ represents the material's polarization in response to the field, while the imaginary part $\varepsilon_2(\omega)$ corresponds to absorption and electronic transitions. Although these two components might appear distinct, they are inherently linked through the Kronig-Kramers relation (Luo *et al.*, 2022). Figures-2(a & b) respectively represent the imaginary and real component of dielectric function of $MoTe_2$ and $MoSe_2$ materials. In both figures, dielectric function has been computed along xx-, yy- and zz-directions, and the curves in x- and y-directions are equal to one another due to their symmetric nature. In figure 2(a), the sharp peaks are appeared correspond to their inter-band electronic transitions. The primary peak for x = y- and z-directions are found at 2.27 eV and 4.65 eV respectively. They are seen mostly within the visible and ultraviolet region. This data suggests stronger electronic transitions in x = y-direction than in the z-direction. Moreover, peaks in x = y- and z-direction at 2.27 eV and 4.65 eV suggested that the highest optical absorption of materials are occurred at these energies for the materials. Zero value of $\varepsilon_{xx}(\omega)$ and $\varepsilon_{yy}(\omega)$ in range (0.00 - 1.01) eV of considered materials could be attributed to topmost occupied electron levels. Same is the case for $\varepsilon_{zz}(\omega)$ upto 2.16 eV. Also, the energy above 8 eV, electrons play no significant part in optical spectrum. Figure-2(b) illustrated the real component of dielectric function. The static dielectric constants $\varepsilon_1(0)$ for x = y, and z-directions are found to be 7.5 and 2.8. The maximum and minimum value of $(Real\ \varepsilon_1(\omega))$ dielectric function in x = y-directions are found to be 11.8 and -3.21 respectively, while in z-direction they are found to be 5.40 and -1.65. Here, the negative values of $\varepsilon_{xx}(\omega)$, $\varepsilon_{yy}(\omega)$ & $\varepsilon_{zz}(\omega)$ indicate that electric field vector and electric displacement vector appeared in opposite direction. Moreover, when the features in the dielectric function are connected to specific electronic transitions in the band structure of the considered compounds, the strong peaks in the imaginary part $\epsilon_2(\omega)$ arise from transitions between the VBM and CBM (critical point transitions). These transitions account for the pronounced optical response and in the visible and ultraviolet region, while the diminishing $\epsilon_2(\omega)$ at higher photon energies indicates fewer allowed transitions at higher conduction bands.

Additionally, both monolayer $MoTe_2$ and $MoSe_2$ exhibits $\varepsilon_1(\omega) > 0$, and $\varepsilon_2(\omega) \sim 0$ in infrared region, suggesting that the materials are transparent in IR region. This is because light passes through the material without significant attenuation and minimal absorption. Higher $\varepsilon_{xx}(0)$ and $\varepsilon_{yy}(0)$ indicate greater polarizability in the x-y plane than along z. Also, in both figures 2(a & b), $\varepsilon_{xx}(\omega) = \varepsilon_{yy}(\omega) \neq \varepsilon_{zz}(\omega)$ implies the materials are optically anisotropic in nature. Similarly, electrons above the 8 eV energy do not have any significant role in optical spectrum.

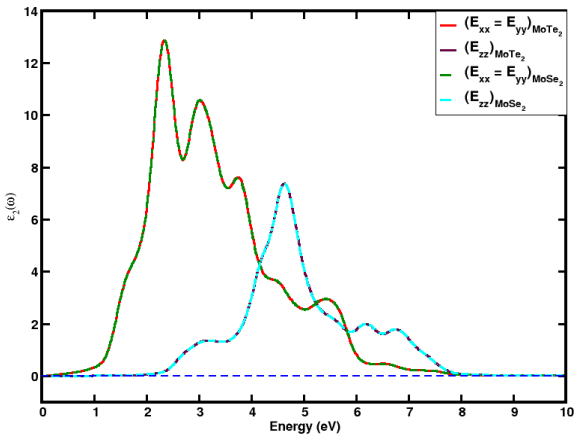

(a)

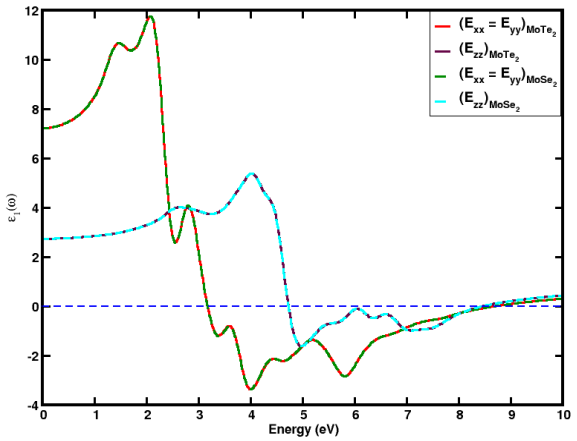

(b)

Figure 2. (Color online) The variation of dielectric function with the corresponding energy value of $MoSe_2$ and $MoTe_2$ materials;(a) Imaginary part of complex dielectric function, and (b) Real component of dielectric function.

From the above obtained dielectric function plots of $MoTe_2$ and $MoSe_2$ materials, it is concluded that the optical curves of both materials have almost equal and mostly overlap with each other in all energy ranges, which is due to the close band gap energy values of materials.

Optical Conductivity

Optical conductivity characterizes the electronic response of a material under the influences of external electromagnetic field. It essentially measures how well the materials conducts electricity when exposed to the such field. Similar to dielectric function, optical conductivity of materials is expressed in the sum of real and imaginary parts, which is given by the relation (11) (Luo *et al.*, 2022; Neupane & Adhikari, 2020);

$$\sigma(\omega) = \sigma_1(\omega) + i\sigma_2(\omega) \quad \ldots (11)$$

Optical conductivity and dielectric of materials are interconnected to each other, where the imaginary part of optical conductivity $\sigma_2(\omega)$ is related to real part of the dielectric function while, real component of optical conductivity $\sigma_1(\omega)$ is connected to imaginary part of dielectric function. The figure 3 illustrated the complex optical conductivity of $MoTe_2$ and $MoSe_2$ monolayer materials. Similar to dielectric function plot, the data for both materials are shown considerable overlap. The graph shows that $\sigma_2(\omega)$ starts at zero and then gradually decreases to minimum of value -6.98 $\Omega^{-1}m^{-1}$ at 2.1 eV. After that it is gradually increasing to up to zero value at 3.07 eV, and remains positive for higher energy values. This data shows that zero value is due to absence of free charge carriers at low energy, the negative imaginary part of the optical conductivity (σ_2) reflects the material's dielectric response and phase lag between current and applied field. The graph of $\sigma_1(\omega)$ is quite similar to the curve of imaginary part of dielectric function $\varepsilon_2(\omega)$, in x- and y- direction. As we can see, the value of $\sigma_1(\omega)$ is zero in range (0.00 - 1.10) eV, indicating that there is no absorption, which is due to the lack of electronic transitions at these energy regions. Beyond this point, the curves are increased sharply with multiples peaks in the energy range of values (2.20 – 3.80) eV, after which it begins to decline. The highest peak for both materials appeared at 3.06 eV, which lies within the visible energy region. These results are comparable with the reported value of other materials (Ruppert *et al.* 2014). These peaks in $\sigma_1(\omega)$ are a result of inter-band transitions between occupied and unoccupied states. The peaks of materials are also implying the higher absorption energy (and hence, higher potential) in transferring light in that energy range and deeper penetration of electromagnetic waves. But, decrease in the value of $\sigma_1(\omega)$ from 3.8 eV is caused by reduced inter-band transition as there are limited number of carriers present. The zero value of optical conductivity ($\sigma_1(\omega)$ and $\sigma_2(\omega)$) at low energy region is a good indication that both monolayer $MoTe_2$ and $MoSe_2$ behaves as semiconductor.

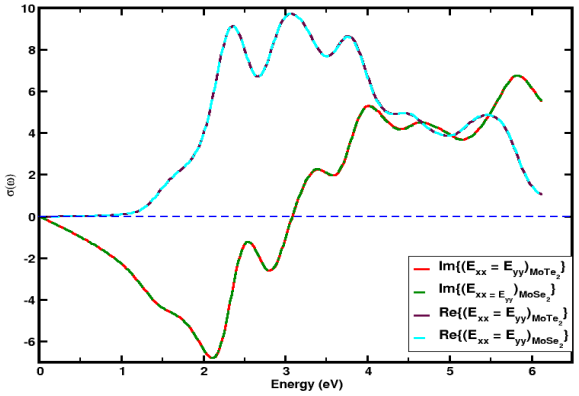

Figure 3. (Color online) Complex optical conductivity (σ) of $MoSe_2$ and $MoTe_2$ monolayer supercell structures, where the graph has been plotted against energy. Here, "Im" denotes imaginary component of σ and "Re" denotes real component of σ .

Optical Coefficients

Here, we have analyzed the three types of optical coefficients that is absorption coefficient $\alpha(\omega)$, transmission coefficient (T%) and reflection coefficient $R(\omega)$ using the values of dielectric function. Absorption coefficient is used to study intensity loss of electromagnetic wave as it traverses through the medium. Figure 4(a) shows the frequency dependent

absorption coefficient α(ω) curve for $MoTe_2$ and $MoSe_2$ materials. It is seen that the optical coefficient curves of $MoTe_2$ and $MoSe_2$ are almost same. Here, the value of α(ω) starts at 1.10 eV and begins to rising rapidly at visible light region, which is due to the phonon energy at that energy range becomes higher than absorption edge region. Hence, $MoTe_2$ and $MoSe_2$ has good absorption coefficient in the visible region. The absorption edge of the materials shifts toward the UV region, which is attributed to the higher photon energy at these absorption edges. Hence, fewer photons are absorbed at the absorption edge, and the curve starts decreasing. This type of responses is typically found in the semiconducting materials. Moreover, zero value of α(ω) is found at 0 eV photon energy value. The low energy value indicates that the considered materials are said to be semiconductors, which also provides further evidence to our result obtained from optical conductivity plots. We know that transmission coefficient is given by the equation (12);

$$T = 1 - A - R \ldots (12)$$

Where, T is a transmission coefficient, A is an absorption coefficient, and R is a reflection coefficient (reflectivity). Here, T depends on thickness of the material. Figure 4(b) shows the computed energy dependent transmittance spectra (in %) of monolayer $MoTe_2$ & $MoSe_2$ materials. The transmittance is found to be 100% up to 1.2 eV energy value. The zero value of α(ω), R(ω), and 100 % value of transmission coefficient (T) at the IR region indicated that materials have transparent properties in the IR region. However, in the visible light, and early UV region, the absorption and reflection coefficient of materials start increasing, and transmittance coefficient (T%) begins decreasing. The T% starts to grow again after 4 eV as α(ω) and R(ω) start to plummet. Figure 4(c) shows the reflectivity spectrum for monolayer $MoSe_2$ and $MoTe_2$. As is evident, R(ω) is zero until ~0.5 eV, after which the curve starts rising at a rapid pace and reaches the maximum value of ~1.07 at visible light region. Apart from that, R(ω) has many peaks at visible region and UV region, which is suggested that materials can be used in filtering or waveguiding applications within the (1.60 – 4.00) eV range. As energy increases further, reflectivity falls and transmittance increases, which is consistent with decreasing absorption and wave interaction at higher photon energies, as shown in the figure 4.

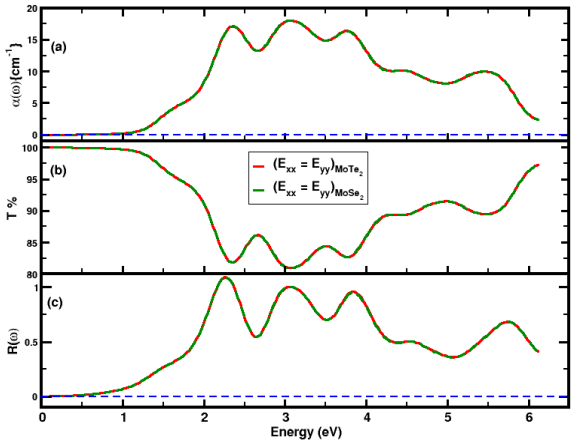

Figure 4. (Color online) (a) Absorption coefficient α(ω), and (b) Transmittance (in %), and (c) Reflectivity R(ω). All parameters are plotted against photon energy.

CONCLUSIONS

We have investigated the mechanical, thermal, and optical properties of (3×3) supercell structures of $MoTe_2$ and $MoSe_2$ monolayer materials. All calculations were performed using the DFT method implemented in Quantum ESPRESSO. The GGA with PBE functional was employed to compute the exchange-correlation energy. The mechanical properties of $MoTe_2$ and $MoSe_2$ were studied through analysis of their elastic constants and moduli of rigidity. Based on the Young's modulus, Bulk modulus, and Shear modulus, we found that $MoTe_2$ and $MoSe_2$ are soft to moderately stiff materials and exhibit anisotropic behavior. For thermal properties, we analyzed the phonon velocities and Debye temperatures of $MoTe_2$ and $MoSe_2$. $MoTe_2$ was found to have a lower phonon velocity than $MoSe_2$, indicating that it conducts heat less efficiently and has softer lattice vibrations. The calculated Debye temperatures (θ_D) are 114.90 K for $MoTe_2$ and 135.20 K for $MoSe_2$, suggesting that $MoSe_2$ has superior thermal properties. The smaller θ_D of $MoTe_2$ also reflects weaker bonding and a lower specific heat capacity compared to monolayer $MoSe_2$. Optical properties were predicted based on the materials' complex dielectric function. Both $MoTe_2$ and $MoSe_2$ exhibit optical anisotropy, with a greater degree of polarization in the x and y directions than in the z direction. We also studied the materials' complex optical conductivity, transmittance, and reflectivity spectra. High transmission occurs in the low-energy region (up to ~1.2 eV), while strong absorption is observed in the range (1.10-3.5) eV. This indicates that both materials are transparent in the lower and mid-infrared (IR) regions but are good absorbers in the higher infrared and visible regions. Based on these optical properties, $MoTe_2$ and $MoSe_2$ show potential

for applications in efficient solar cells, electromagnetic shielding, and various optoelectronic devices.

ACKNOWLEDGMENTS

The authors would like to thank the Condensed Matter Research Lab CDP TU, TWAS Research Funds RG 20-316, Network Project NT-14 of ICTP/OE for the computing capacity, and Prof. NP Adhikari for his constructive suggestions on the manuscript.

AUTHOR CONTRIBUTIONS

Conceptualization: TN, HKN; Investigation: TN, AP, KK, SKY, TN, GP, OSR; Methodology: TN, AP, KK, SKY, TN, GP and OSR; Data curation: HKN; Data analysis: HKN; Writing - original draft: TN; Writing - review and editing: TN, AP, KK, SKY, TN, GP, OSR.

CONFLICT OF INTEREST

The authors declare no conflicts of interest.

DATA AVAILABILITY STATEMENT

The corresponding author can provide the data used to prepare figures and tables on the request of publisher.

REFERENCES

Al-Qaisi, S., Abu-Jafar, M., Gopir, G., Ahmed, R., Omran, S. B., Jaradat, R., Khenata, R. (2017). Structural, elastic, mechanical and thermodynamic properties of terbium oxide: First-principles investigations. *Results in Physics*, 7, 709-714.

Anderson, O. L. (1963). A simplified method for calculating the Debye temperature from elastic constants. *Journal of Physics and Chemistry of Solids*, 24(7), 909-917.

Aryal, S., Paudel, G., Nepal, M., Oli, D., Rijal, O. S., & Neupane, H. K. (2025). Water Adsorption on Pristine and Vacancy Defected h-BN Monolayer: First-principles Study. *Journal of Institute of Science and Technology*, 30(1), 73-81.

Baithi, M., & Duong, D. L. (2024). Doped, Two-Dimensional, Semiconducting Transition Metal Dichalcogenides in Low-Concentration Regime. *Crystals*, 14(10), 832.

Bartolotti, L. J., & Flurchick, K. (1996). An introduction to density functional theory. *Reviews in Computational Chemistry*, 187-216.

Brown, B. E. (1966). The crystal structures of WTe2 and high-temperature MoTe2. *Acta Crystallographica*, 20, 268-174.

Chang, Y. M., Lin, C. Y., Lin, Y. F., & Tsukagoshi, K. (2016). Two-dimensional MoTe2 materials: From synthesis, identification, and charge transport to electronics applications. *Japanese Journal of Applied Physics*, 55(11), 1102A1.

Chen, Z., Gandhi, U., Lee, J., & Wagoner, R. H. (2016). Variation and consistency of Young's modulus in steel. *Journal of Materials Processing Technology*, 227, 227-243.

Cohen, M. L. (1985). Calculation of bulk moduli of diamond and zinc-blende solids. *Physical Review B*, 32(12), 7988.

Dal Corso, A. (1996). A pseudopotential plane waves program (pwscf) and some case studies. *Quantum-mechanical Ab-initio Calculation of the Properties of Crystalline Materials*, 155-178. Berlin, Heidelberg: Springer Berlin Heidelberg.

D'angelo, M., & Matsuda, I. (2019). *Monatomic Two-Dimensional Layers*. Elsevier.

Giustino, F. (2014). Materials modelling using density functional theory: Properties and Predictions. *Oxford University Press*.

Han, D., Qin, H., Tu, H., Chen, Y., Sun, H., Xue, Y., & Zeng, X. (2025). Comparative Analysis of Phonon Thermal Transport Properties in 2D Janus TMDC Monolayers: Insights from First-Principles Calculations. *Journal of Electronic Materials*, 54(3), 2180-2191.

Kanoun, B. M. (2018). Tuning magnetic properties of two-dimensional $MoTe_2$ monolayer by doping 3d transition metals: Insights from first principles calculations. *Journal of Alloys and Compounds*, *748*, 938-942.

Kohn, W., & Sham, L. J. (1965). Self-consistent equations including exchange and correlation effects. *Physical Review*, *140*(4A), 1133.

Kokalj, A. (2003). Computer graphics and graphical user interfaces as tools in simulations of matter at the atomic scale. *Computational Materials Science*, *28*(2), 155-168.

Komatitsch, D., Vilotte, J.-P., Vai, R., Castillo-Covarrubias, J. M., & Sanchez-Sesma, F. J. (1999). The spectral element method for elastic wave equations—application to 2-d and 3-d seismic problems. *International Journal for Numerical Methods in Engineering*, *45*(9), 1139-1164.

Körner, W., & Elsässer, C. (2010). First-principles density functional study of dopant elements at grain boundaries in ZnO. *Physical Review B-Condensed Matter and Materials Physics*, *81*(8), 085324.

Kuc, A., Heine, T., & Kis, A. (2015). Electronic properties of transition-metal dichalcogenides. *MRS Bulletin*, *40*(7), 577-584.

Kumar, V. P., Raut, P., Panda, D. K., & Rashed, A. N. Z. (2025). Exploring Next Generation TMDC Materials: A Comprehensive Review of Their Classifications, Properties, and Applications. *Silicon*, 1-23.

Li, Y., Feng, Z., Sun, Q., Ma, Y., Tang, Y., & Dai, X. (2021). Electronic, thermoelectric, transport and optical properties of MoSe2/BAs van der Waals heterostructures. *Results in Physics*, *23*, 104010.

Lin, Z., Yang, X., He, J., Dong, N., & Li, B. (2025). Structural and optoelectronic characterization of anisotropic two-dimensional materials and applications in polarization-sensitive photodetectors. *Applied Physics Reviews*, *12*(1), 011301.

Luo, Z., Hao, J., & Li, J. (2022). The optical properties of $MoSe_2$ in bulk and monolayer with different crystal orientation based on first-principles calculations. *Academic Journal of Materials & Chemistry*, *3*(1), 51-57.

Ma, Y., Dai, Y., Guo, M., Niu, C., Lua, J., & Huanga, B. (2011). Electronic and magnetic properties of perfect, vacancy-doped, and nonmetal adsorbed $MoSe_2$, $MoTe_2$ and WS_2 monolayers. *Physical Chemistry Chemical Physics*, *13*, 15546-15553.

Mia, A. K., Meyyappan, M., & Giri, P. (2023). Two-dimensional transition metal dichalcogenide based biosensors: from fundamentals to healthcare applications. *Biosensors*, *13*, 169.

Mouhat, F., & Coudert, F. X. (2014). Necessary and sufficient elastic stability conditions in various crystal systems. *Physical Review B*, *90*(22), 224104.

Nakamura, K. (2018). First-principles simulation on thermoelectric properties of transition metal dichalcogenide monolayers. *Japanese Journal of Applied Physics*, *57*(6S1), 06HE04.

Nepal, M., Paudel, G., Aryal, S., Devkota, A., & Neupane, H. K. (2024). Adsorption of water on vacancy defective h-bn bilayer at b and n sites: First-principles calculation. *Bibechana*, *21*(2), 129-141.

Neupane, H. K., & Adhikari, N. P. (2020). Structure, electronic and magnetic properties of 2D Graphene-Molybdenum diSulphide (G-MoS_2) Heterostructure (HS) with vacancy defects at Mo sites. *Computational Condensed Matter*, 24, e00489.

Neupane, H. K., & Adhikari, N. P. (2020). Tuning Structural, Electronic, and Magnetic Properties of C Sites Vacancy Defects in Graphene/MoS2 van der Waals Heterostructure Materials: A First-Principles Study. *Advances in Condensed Matter Physics*, 2020(1), 8850701.

Neupane, H. K., & Adhikari, N. P. (2021). Electronic and magnetic properties of defected MoS2 monolayer. *BIBECHANA*, *18*(2), 68-79.

Novoselov, Kostya, S., Jiang, D., Schedin, F., Booth, T., Khotkevich, V., & Geim, A. (2005). Two-dimensional atomic crystals. *Proceedings of the National Academy of Sciences*, *102*, 10451-10453.

Orio, M., Pantazis, D. A., & Neese, F. (2009). Density functional theory. *Photosynthesis Research*, *102*, 443-453.

Lawaetz, P. (1972). Stability of the wurtzite structure. *Physical Review B*, *5*(10), 4039.

Pathak, A. (2019). Effect of Cr on electronic and mechanical properties of TiS2 compound: A first-principles study. *Journal of Applied Research and Technology*, *17*(4), 302-312.

Paudel, G., Nepal, M., Aryal, S., Devkota, A., & Neupane, H. K. (2023). Effect of water adsorption on bilayer h-bn: First-principles study. *Journal of Nepal Physical Society*, *9*(2), 56-62.

Pumera, Z. S. (2014). Layered transition metal dichalcogenides for electrochemical energy generation and storage. *Journal of Materials Chemistry*, *2*, 8981-87.

Puotinen, D., & Newnham, R. (1961). The crystal structure of molybdenum ditelluride. *Acta Crystallographica*, *14*, 691-692.

Rassay, S. S. (2017). Electrical, electronic and optical properties of $MoSe_2$ and WSe_2. *New Jersey Institute of Technology*.

Reuss, A. J. Z. A. M. M. (1929). Calculation of the flow limits of mixed crystals on the basis of the plasticity of monocrystals. *Zeitschrift für Angewandte Mathematik und Mechanik*, *9*(1), 49-58.

Rijal, O. S., Neupane, H. K., Oli, D., Neupane, R. K., Shrestha, P., Sharma, S., ... & Parajuli, R. (2025). A first-principles investigation of the structural, mechanical, dynamic, electronic, magnetic, and optical properties of Ti2AC (A= Cd, S) MAX phase compounds. *Journal of Physics D: Applied Physics*, 58(12), 125102.

Ruppert, C., Aslan, O. B., & Heinz, T. F. (2014). Optical Properties and Band Gap of Single- and Few-Layer $MoTe_2$ Crystals. *Nano Letters*, 14(11), 6231-6236.

Tsai, M. L., Su, S. H., Chang, J. K., Tsai, D. S., Chen, C. H., Wu, C. I., ... & He, J. H. (2014). Monolayer MoS_2 heterojunction solar cells. *ACS Nano*, *8*(8), 8317-8322.

Tongay, S., Zhou, J., Ataca, C., Lo, K., Matthews, T.S., Li, J., Grossman, J.C., & Wu, J. (2012). Thermally driven crossover from indirect toward direct bandgap in 2d semiconductors: $MoSe_2$ versus MoS_2. *Nano Letters*, *12*(11), 5576-5580.

Van Voorhis, T., & Scuseria, G. E. (1998). A novel form for the exchange-correlation energy functional. *The Journal of Chemical Physics*, *109*(2), 400-410.

Vellinga, M., De Jonge, R., & Haas, C. (1970). Semiconductor to metal transition in molybdenum ditelluride. *Journal of Solid State Chemistry*, *2*(2), 299–302.

Wang, Q. H., Kalantar-Zadeh, K., Kis, A., Coleman, J. N., & Strano, M. S. (2012). Electronics and optoelectronics of two-dimensional transition metal dichalcogenides. *Nature Nanotechnology*, *7*(11), 699-712.

Wang, Y., Wisesa, P., Balasubramanian, A., Dwaraknath, S., & Mueller, T. (2021). Rapid generation of optimal generalized Monkhorst-Pack grids. *Computational Materials Science*, *187*, 110100.

Zeng, F., Zhang, W. B., & Tang, B. Y. (2015). Electronic structures and elastic properties of monolayer and bilayer transition metal dichalcogenides MX2 (M= Mo, W; X= O, S, Se, Te): a comparative first-principles study. *Chinese Physics B*, *24*(9), 097103.